

AFM-Based Quantification of Conformational Changes in DNA Caused by Reactive Oxygen Species

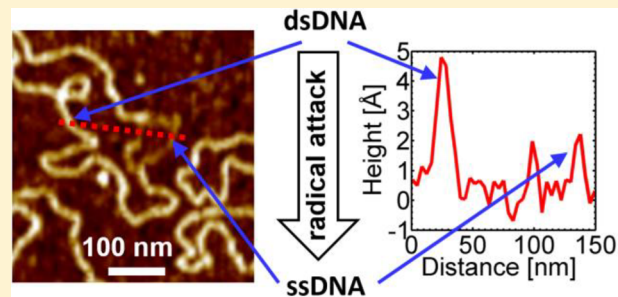
Florian Berg,[†] Janine Wilken,[†] Christiane A. Helm,^{*,†} and Stephan Block^{*,†,‡}

[†]Institut für Physik, Ernst-Moritz-Arndt Universität, Felix-Hausdorff-Strasse 6, D-17487 Greifswald, Germany

[‡]Department of Applied Physics, Chalmers University of Technology, SE-41296 Gothenburg, Sweden

Supporting Information

ABSTRACT: Radical induced modification of DNA plays an important role in many pathological pathways like cancer development, aging, etc. In this work, we quantify radical-induced DNA damage that causes transitions from double to single stranded DNA using atomic force microscopy (AFM). The plasmid pBR322 is attacked by free hydroxyl radicals that are produced by Fenton's reaction; the strength of the radical attack is controlled via the ratio of hydroxyl radical molecules to DNA base pairs. The extent of DNA modification is assessed by AFM tapping mode (TM) imaging of the plasmids (after adsorption onto PAH-functionalized mica) in air. As single stranded DNA chains (height $\sim 2 \text{ \AA}$) are much smaller than intact DNA strands ($\sim 5 \text{ \AA}$), their fraction can be quantified based on the height distribution, which allows a simplified data analysis in comparison to similar AFM-based approaches. It is found that the amount of damaged DNA strands increases with increasing strength of radical attack, and decreases if ROS scavengers like sodium acetate are added. Competition curves are calculated for the interaction of hydroxyl radicals with DNA and sodium acetate, which finally allows calculation of relative rate constants for the respective reactions.



INTRODUCTION

Biological systems are constantly exposed to reactive oxygen species (ROS), which are produced by exogenous sources like carcinogenic compounds and ionizing irradiation, but also by endogenous sources as part of the normal oxidative metabolism or immune responses (e.g., ROS release from phagocytic cells). It is well established that ROS, especially hydroxyl radicals, are able to induce a variety of DNA modifications, which might be categorized based on their chemical impact (e.g., chemical sugar and base modifications, single and double strand breaks, formation of DNA–DNA or DNA–protein cross-links) or physical outcome (e.g., conformational changes from supercoiled into relaxed configurations, transitions from double to single stranded chains).^{1–4} Hence, ROS play an important role in many pathological pathways, in cancer development, aging, etc.^{5–7}

Investigation of ROS–DNA interactions requires methods that allow an accurate quantification of ROS-induced DNA damage. In the past, many methods have been developed that are able to quantify DNA damage from different points of view. Approaches that combine chromatography and mass spectrometry offer highest resolutions with the ability to detect DNA damage in terms of chemical modifications on the level of single sugars and bases.^{2,8} However, these approaches require quite complex sample preparations, which themselves might induce ROS-related DNA damage. Moreover, as hydrolyzation of the base pairs is usually a requirement for application of these approaches, they are mostly insensitive to conformational

changes of the whole DNA strand, modifications that are known to have high potential to enhance mutagenicity.³ Such conformational changes can be studied with gel electrophoretic approaches, which are able to separate damaged DNA strands based on differences in strand size, conformation, and charges.⁹ However, as the migration behavior of the strands is influenced by each of these properties, a direct interpretation of the gel electrophoretic results becomes difficult if the strands form a heterogeneous mixture, i.e., if the ROS induced DNA modifications differ from one strand to the next.

Among the approaches offering single molecule detection, atomic force microscopy (AFM) proved very useful to study radical–DNA interaction, as it allows visualization of ROS-induced conformational changes of individual DNA strands, yielding complementary information to the approaches introduced above. Most AFM studies published so far image radical-attacked DNA after immobilization to a surface and quantify either the transition from the supercoiled into relaxed conformations (which is indicative for single strand breaks) or the extent of DNA strand fragmentation as result of double strand breaks.^{10,11} Here, we introduce a new quantification approach, which takes advantage of the fact that the diameter of a single strand is smaller than the diameter of double strands. As a consequence, single strands exhibit smaller heights in AFM

Received: July 30, 2014

Revised: November 9, 2014

Published: December 3, 2014

imaging than double strands,¹² enabling calculation of the ratio between the surface coverage of single and double strands. This allows determination of the fraction of the DNA strand that underwent a transition from double to single strand conformation due to the interaction with radicals and therefore assessment of the extent of ROS-induced DNA damage that causes conformational changes of the DNA. Finally, the approach is applied to quantify the inhibition of radical attacks by scavengers.

MATERIALS AND METHODS

Materials. The circular plasmid DNA pBR322 (4361 bp) was purchased from Carl Roth (Karlsruhe, Germany). Poly(allylamine hydrochloride) (PAH, $M_w = 58$ kDa) and sodium acetate (NaOAc) were obtained from Sigma-Aldrich (München, Germany). Fenton's reagent is made from EDTA (ethylenediaminetetraacetic acid, Sigma-Aldrich), Mohr's salt (ammonium iron(II) sulfate, Merck, Darmstadt, Germany), and H_2O_2 (hydrogen peroxide, Roth, Karlsruhe, Germany). The molar ratio between EDTA, Fe^{2+} , H_2O_2 , and NaOAc is specified in Section S1 of the Supporting Information. All chemicals are of analytical grade and are used without further purification. All solutions are prepared with deionized, ultrapure water using a Milli-Q water purification device (Millipore, Billerica, MA).

Mica (surface roughness <1 Å; Nanoscience Instruments, Phoenix, AZ) serves as negatively charged substrate for the AFM measurements. All AFM tapping mode images are recorded with a DI Multimode and a Nanoscope IIIa controller (Digital Instruments, Santa Barbara, CA). For AFM imaging OMCL-AC160TS Cantilevers (spring constant $k = 42$ N/m, radius of curvature $r_c \cong 8$ nm) from Olympus Corporation (Hamburg, Germany) are used.

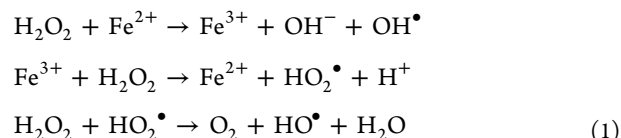
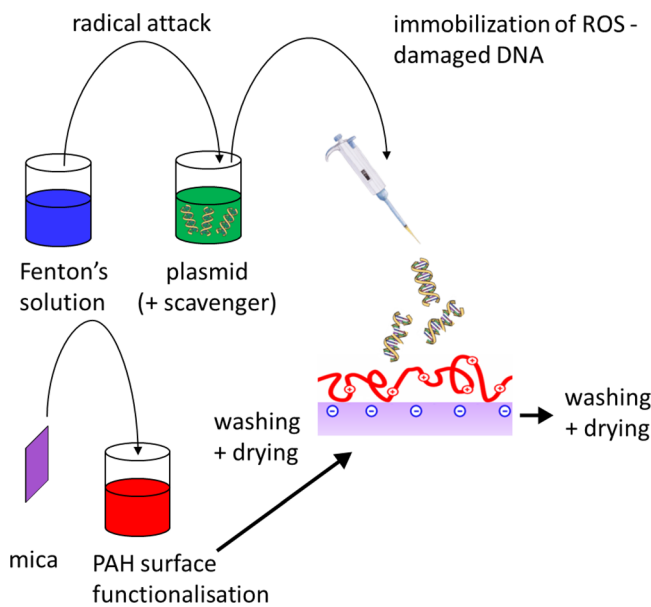
Sample Preparation. For surface functionalization freshly cleaved mica sheets are immersed into 3 mM (with respect to the monomer concentration) PAH solution for 45 min, as shown in Scheme 1. After washing the functionalized sheets under running Milli-Q water, they are dried in a laminar flow box (BDK Luft- und Reinraumtechnik GmbH, Sonnenbühl-Genkingen, Germany).

To generate hydroxyl radicals (using Fenton's reaction as shown in eq 1)^{13,14} a pipet with H_2O_2 solution is drained into a beaker with Fe^{2+} -EDTA solution. Immediately afterward, the same pipet is used to transfer a defined volume, as indicated in Section S1 of the Supporting Information, into a second beaker containing 0.12 mM (with respect to the nucleotide concentration) pBR322 DNA solution and H_2O . After a reaction time of 5 min, the content of the second beaker is brought onto the dried PAH surface by placing a drop of the radical-attacked DNA solution onto the PAH-functionalized mica surface. After 50 s adsorption time, the nonadsorbed material is washed off using running Milli-Q water and the sample is dried in the laminar flow box.

In the case of the DNA protection using ROS scavengers, the second beaker is filled with a mixture of DNA and sodium acetate (NaOAc) of different ionic strengths as indicated in Section S1 of the Supporting Information. Using a pipet Fenton's reagent is transferred to this second beaker as described in the section above.

We have generated ROS with the help of the Fenton reaction:

Scheme 1. Immobilization of DNA after Radical Attack onto PAH-Functionalized Mica for AFM Tapping Mode Imaging in Air



The strength of radical attack is varied by variation of H_2O_2 concentration $c_{H_2O_2}$ (ranging between 0.43 mM and 1.30 mM) as indicated in Section S1 of the Supporting Information.

AFM Imaging and Quantification of DNA damage. Imaging of DNA adsorbed onto PAH surfaces is performed using AFM tapping mode in air. Every sample is imaged at three different $2 \times 2 \mu\text{m}^2$ areas. Typically, we observe a mixture of single and double stranded DNA chains (ssDNA and dsDNA, respectively) that are immobilized on the PAH-functionalized mica (see Figure 1 for an exemplary measurement containing DNA damage that causes partial splitting of dsDNA chains into ssDNA ones).

For quantification of the DNA damage causing a transition from dsDNA to ssDNA, a home-written script in MatLab (MathWorks, Natick, MA) uses the height of the AFM tapping mode image, i.e., the pixels are categorized according to their height h as exemplarily shown in the cross sections of Figure 1d. The approach is based on the observation that a dsDNA chain exhibits a chain height of approximately 5 Å after immobilization on PAH, while ssDNA reaches only 2 Å (see Supporting Information regarding the reproducibility of the dsDNA and ssDNA height in our experiments). Hence, choosing a height threshold between the dsDNA and ssDNA chain height allows an automatic identification of these pixels, which are occupied by dsDNA chain segments. Similarly, pixels corresponding to ssDNA chains (resulting from the radical attack of the dsDNA chain) are identified using a height threshold between the ssDNA chain height and the root mean squared roughness of the PAH-functionalized mica (≤ 0.8 Å). Finally, a pixel height $h < 0.8$ Å evidences the PAH background and $h > 8$ Å is associated with contaminations on the PAH

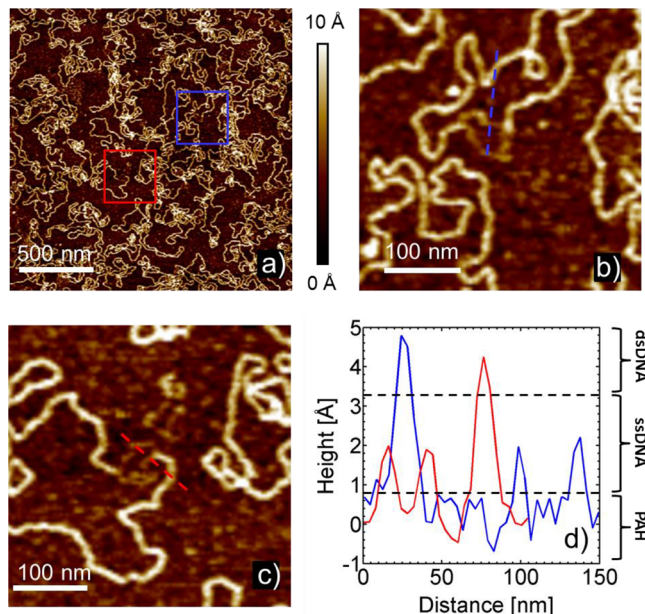


Figure 1. (a) Representative AFM tapping mode image ($2 \times 2 \mu\text{m}^2$; colored scale bar indicates height) of DNA after radical attack at $c_{\text{H}_2\text{O}_2} = 0.43 \text{ mM}$, adsorbed onto PAH-functionalized mica. The two colored rectangles are enlarged in panels b and c. Both zoom images show a double stranded DNA (dsDNA), which splits (due to radical damage) into two single stranded DNAs (ssDNA). The cross section of the colored dashed lines is given in panel d. We typically observe a dsDNA chain height of approximately 5 Å, while ssDNA reaches only 2 Å. Hence, areas occupied by dsDNA can be easily distinguished from ssDNA or empty areas using a categorization algorithm based on the pixel height in the respective areas (the black dashed lines in panel d represent the height thresholds used for this categorization).

surface; both events are not considered in the further quantification.

Since the height of a single strand is only slightly above the PAH background, additional data transformations are necessary for an accurate quantification of the surface coverage of the ssDNA. Figure 2a shows a $2 \times 2 \mu\text{m}^2$ AFM image (512×512 pixels) and a 10×10 matrix containing notional values, which symbolizes the pixel height h . Figure 2b shows the color coded height image of Figure 2a and the corresponding color coded matrix according to the associated color bar. All pixels with a height of $h < 0.8 \text{ \AA}$ are interpreted as the supporting PAH-functionalized surface and are therefore set to $h = 0 \text{ \AA}$.

The MatLab script laterally counts contiguous pixels that exceed the value $h > 0.8 \text{ \AA}$. Events having areas of less than about 50 pixels, which corresponds to a contour length of 40–50 nm being equivalent to 120–150 bp (assuming the DNA chain has a width of 4–5 pixels, 15–20 nm, see Figure 1d),^{15,16} are associated with the PAH background and excluded from further quantification. An almost noise-free image, as depicted in Figure 2c, results from this procedure.

The percentage fraction of damaged plasmid $F_{\text{DNA,d}}$ (i.e., the fraction of the DNA chain that underwent a transition to single strands) can be determined by counting “blue” (dsDNA, $3.3 \text{ \AA} < h < 8 \text{ \AA}$) and “yellow” (ssDNA, $0.8 \text{ \AA} < h < 3.3 \text{ \AA}$) pixels, respectively, and by applying eq 2.

$$F_{\text{DNA,d}} = \frac{a_d}{a_d + a_i} \times 100 \quad (2)$$

Here, a_d and a_i are the dsDNA and ssDNA areas, respectively. The dsDNA area a_d can be directly associated with the product of pixel size area, A_p , and the number of pixels P_d corresponding to intact plasmid, $a_d = P_d A_p$. However, care has to be taken in the determination of a_d as (due to AFM tip convolution) even “completely intact DNA strands” are surrounded by a yellow edge area, indicative of decreased height, erroneously suggesting DNA damage (see, e.g., the matrix of Figure 2c for a representative example). This leads to an overestimation of the ssDNA area a_d if directly calculated from the number of pixels P_d corresponding to apparently damaged plasmid. Hence, for the correct quantification of a_d the “edge area” of dsDNA has to be subtracted using $a_d = P_d A_p - a_i \times 0.82$. Here, the factor for correcting the overestimated damaged area is set to 0.82, which was determined from AFM images of completely intact DNA strands that were not subject to any radical attack.

To evaluate the accuracy of this data analysis, synthetic AFM images were created having the same properties (e.g., image size, resolution, etc.) as the AFM images from the experiments. The numerically created AFM images contained DNA chains having a defined fraction of ssDNA chains. A comparison of the results of the data analysis with the (input) values used in the numerics showed that (under our experimental conditions) the data analysis determines the fraction of ssDNA chains $F_{\text{DNA,d}}$ with an accuracy better than 4% points (see Supporting Information for more information on the numerical evaluation).

RESULTS

The plasmid pBR322 is used to investigate the influence of radical oxygen species (ROS) on DNA molecules. The quantification of DNA damage (causing a transition to single DNA strands due to interaction with ROS) is performed by AFM tapping mode imaging of the negatively charged DNA immobilized onto a single, positively charged PAH layer (formed on mica), with or without treating the DNA with ROS before adsorption.

As double and single stranded DNA chains (dsDNA and ssDNA, respectively) adsorb sufficiently flat onto the PAH surface, they can be distinguished by investigating their height as shown in Figure 1d. The height of the dsDNA and ssDNA chains can be measured with high reproducibility (see Supporting Information), and it is observed that dsDNA has approximately twice the height of ssDNA. Hence, height thresholds set between the dsDNA and ssDNA height as well as below the ssDNA height can be used to determine the fraction of dsDNA and ssDNA surface coverage (see Materials and Methods for further information on the quantification process). Assuming that only a double stranded DNA molecule can perform a function, they are considered within this work as an intact DNA. As a single stranded DNA is a clear indication of a radical damage acting on DNA, occurrence of ssDNA is classified throughout this work as damaged DNA. Hence, the extent of DNA damage that causes a transition from double into single strands can be quantified by measuring the fraction of ssDNA to the total DNA amount, which will be denoted by $F_{\text{DNA,d}}$ (eq 2) in the following. Note that $F_{\text{DNA,d}}$ can therefore only reflect those kinds of DNA damage that cause (partial) splitting of DNA into single strands.

Figure 3 shows $1 \times 1 \mu\text{m}^2$ AFM tapping mode images and the corresponding color coded height images of DNA after radical attack immobilized onto PAH-functionalized mica. It is

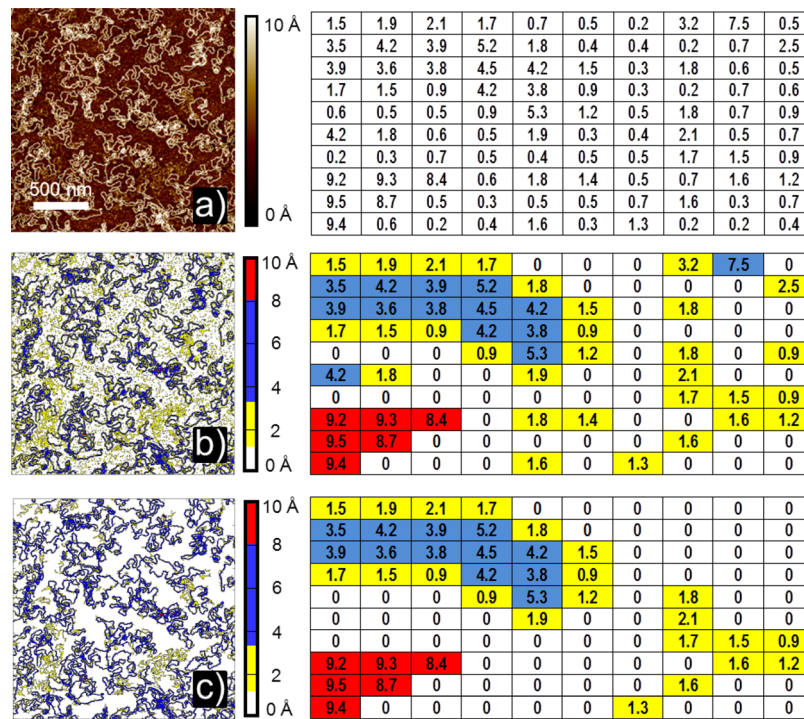


Figure 2. Quantification of DNA damage causing single stranded DNA. (a) An AFM tapping mode image ($2 \times 2 \mu\text{m}^2$) of DNA after radical attack at $c_{\text{H}_2\text{O}_2} = 0.43 \text{ mM}$, adsorbed onto PAH-functionalized mica. The corresponding matrices are meant to show the principle and contain therefore only notional values, which symbolize the pixel height h . (b, c) According to the pixel height, a classification algorithm categorizes each pixel into the following categories as indicated by the color coding of the scale bar: unoccupied area (white, $h < 0.8 \text{ \AA}$), occupied by ssDNA (yellow, $0.8 \text{ \AA} < h < 3.3 \text{ \AA}$), occupied by dsDNA (blue, $3.3 \text{ \AA} < h < 8 \text{ \AA}$), contaminations (red, $h > 8 \text{ \AA}$). (c) For this panel, the PAH background noise is filtered out by removing all “yellow pixels” that are isolated on the surface. Please see Materials and Methods for more details on the classification and filtering algorithm.

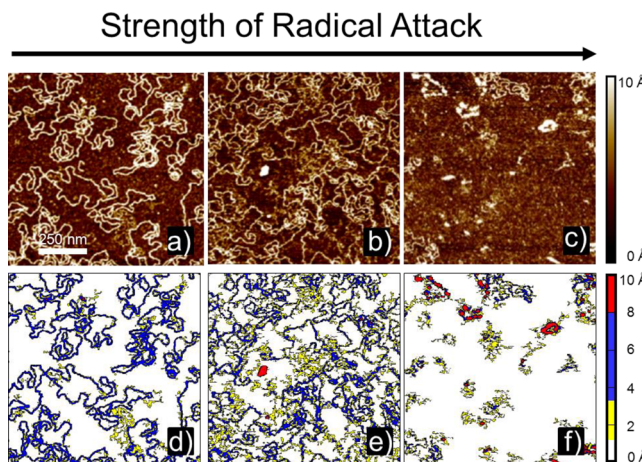


Figure 3. (a–c) AFM tapping mode images ($1 \times 1 \mu\text{m}^2$) of DNA after radical attack adsorbed onto PAH-functionalized mica. The strength of radical attack increases from (a) $c_{\text{H}_2\text{O}_2} = 0.43 \text{ mM}$ to (b) $c_{\text{H}_2\text{O}_2} = 0.87 \text{ mM}$ to (c) $c_{\text{H}_2\text{O}_2} = 1.30 \text{ mM}$. (d–f) These panels show color coded quantification images of same areas (blue = dsDNA, yellow = ssDNA, red = surface contaminations). The percentage fraction of damaged plasmid $F_{\text{DNA,d}}$ (see eq 2) increases from (d) $F_{\text{DNA,d}} = 30.2\%$ to (e) $F_{\text{DNA,d}} = 55.3\%$ to (f) $F_{\text{DNA,d}} = 67.9\%$, which suggests an increasing radical damage of DNA.

apparent from a comparison of Figure 3a–c that the fraction of single stranded DNA monotonously increases from Figure 3a to Figure 3c (Figure 3d–f gives the corresponding color coded images of Figure 3a–c). At $c_{\text{H}_2\text{O}_2} = 0.43 \text{ mM}$ (Figure 3d; blue =

dsDNA, yellow = ssDNA, red = surface contaminations) we find that the radical attack causes $F_{\text{DNA,d}} = 30.2\%$, which increases at $c_{\text{H}_2\text{O}_2} = 0.87 \text{ mM}$ to $F_{\text{DNA,d}} = 55.3\%$ (Figure 3e), and at $c_{\text{H}_2\text{O}_2} = 1.3 \text{ mM}$ to $F_{\text{DNA,d}} = 67.9\%$ (Figure 3f). The monotonously increasing $F_{\text{DNA,d}}$ suggests an increase in radical induced DNA damage with increasing concentration of H_2O_2 .

To further evaluate our quantification approach, we investigated protective effects by adding ROS scavengers to the DNA solution before the radical attack was initiated. Figure 4 shows a series of such measurements, in which sodium acetate (NaOAc) was used as radical scavenger. Figure 4a–c gives $1 \times 1 \mu\text{m}^2$ AFM tapping mode images of DNA immobilized on PAH-functionalized mica after exposure to a mixture of ROS and NaOAc (scavenger concentrations: Figure 4a $c_{\text{NaOAc}} = 2.68 \text{ mM}$, Figure 4b $c_{\text{NaOAc}} = 10.71 \text{ mM}$, Figure 4c $c_{\text{NaOAc}} = 42.86 \text{ mM}$). The strength of the radical attack is fixed by using $c_{\text{H}_2\text{O}_2} = 0.87 \text{ mM}$, which is equivalent to the strength of radical attack shown in Figure 3b,e. Figure 4d–f gives the corresponding color coded images of Figure 4a–c. It is apparent from these images that an increase in scavenger concentration leads to a decrease of the DNA damage: $F_{\text{DNA,d}} = 44.9\%$ (Figure 4d; $c_{\text{NaOAc}} = 2.68 \text{ mM}$), $F_{\text{DNA,d}} = 27.4\%$ (Figure 4e; $c_{\text{NaOAc}} = 10.71 \text{ mM}$), down to $F_{\text{DNA,d}} = 14.6\%$ (Figure 4f; $c_{\text{NaOAc}} = 42.86 \text{ mM}$).

Based on these data, we then investigated if the interplay of ROS and ROS scavenger can be further quantified. Figure 5a gives an overview of the ROS-induced dsDNA to ssDNA transitions for different concentrations of H_2O_2 and NaOAc (as indicated in this figure). Competition curves at fixed strength of

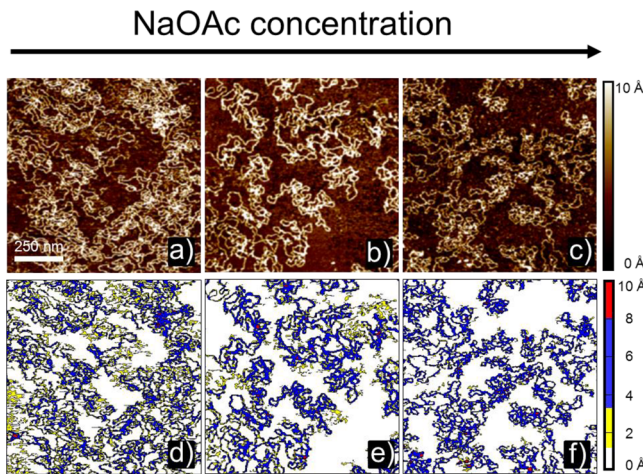


Figure 4. (a–c) AFM tapping mode images ($1 \times 1 \mu\text{m}^2$) of scavenger protected DNA chains after radical attack adsorbed onto PAH-functionalized mica. The concentration of the scavenger increases from (a) $c_{\text{NaOAc}} = 2.68 \text{ mM}$ to (b) $c_{\text{NaOAc}} = 10.71 \text{ mM}$ to (c) $c_{\text{NaOAc}} = 42.86 \text{ mM}$. The strength of radical attack is fixed at $c_{\text{H}_2\text{O}_2} = 0.87 \text{ mM}$. (d–f) These panels show color coded quantification images of the same areas (blue = dsDNA, yellow = ssDNA, red = surface contaminations). The percentage fraction of damaged plasmid $F_{\text{DNA,d}}$ (see eq 2) decreases from (d) $F_{\text{DNA,d}} = 44.9\%$ to (e) $F_{\text{DNA,d}} = 27.4\%$ to (f) $F_{\text{DNA,d}} = 14.6\%$, suggesting a decrease in DNA damage caused by the presence of the scavenger.

radical attack (i.e., for a given H_2O_2 concentration) can be calculated from this figure by normalizing $F_{\text{DNA,d}}$ by its value in the absence of any scavenger, leading to the sigmoidal curves shown in Figure 5b. The experimental data (dots) are fitted according to Hill-like competition model given by eq 3:¹⁷

$$\frac{F_{\text{DNA,d}}}{F_{\text{DNA,d}}(c_{\text{NaOAc}} = 0 \text{ M})} = \frac{1}{1 + \frac{c_{\text{NaOAc}}}{IC_{50}}} \quad (3)$$

Obviously, the $F_{\text{DNA,d}}$ is halved at a scavenger concentration of $c_{\text{NaOAc}} = 10.5 \text{ mM}$ in the case of $c_{\text{H}_2\text{O}_2} = 0.87 \text{ mM}$, which means that 50% of the DNA chains are protected by the scavenger ($IC_{50} = 10.5 \text{ mM}$). For a H_2O_2 concentration of $c_{\text{H}_2\text{O}_2} = 1.3 \text{ mM}$ we observe IC_{50} at 22.1 mM NaOAc.

As in these experiments the hydroxyl radicals interact either with DNA nucleotides or with NaOAc molecules, it is possible to express the fraction of ssDNA, $F_{\text{DNA,d}}$, by

$$\frac{F_{\text{DNA,d}}}{F_{\text{DNA,d}}(c_{\text{NaOAc}} = 0 \text{ M})} = \frac{k_{\text{DNA}} c_{\text{OH}} c_{\text{DNA}}}{k_{\text{DNA}} c_{\text{OH}} c_{\text{DNA}} + k_{\text{NaOAc}} c_{\text{OH}} c_{\text{NaOAc}}} \quad (4)$$

or

$$\frac{F_{\text{DNA,d}}(c_{\text{NaOAc}} = 0 \text{ M})}{F_{\text{DNA,d}}} = 1 + \frac{k_{\text{NaOAc}} c_{\text{NaOAc}}}{k_{\text{DNA}} c_{\text{DNA}}} \quad (5)$$

with k_{DNA} and k_{NaOAc} denoting the rate constants for the interaction of a DNA nucleotide or NaOAc with hydroxyl radicals and c_{DNA} and c_{NaOAc} the respective concentrations. These equations follow directly from the competition kinetics of NaOAc. Assuming that DNA damage causing single strands is a measure for the total amount of DNA damage and using the rate constant for nucleotides known from the literature

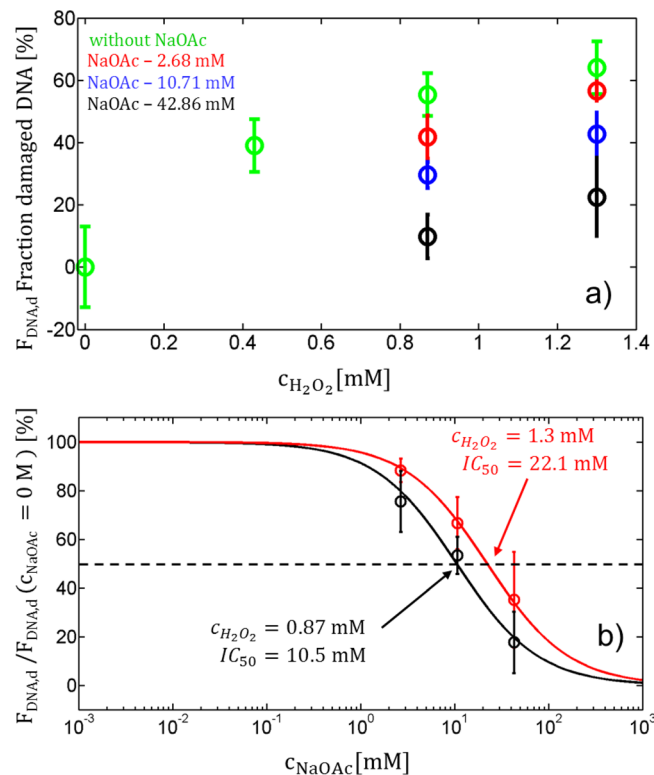


Figure 5. (a) Fraction of ssDNA $F_{\text{DNA,d}}$ versus $c_{\text{H}_2\text{O}_2}$. The green dots show $F_{\text{DNA,d}}$ without protective scavenger; the red, blue, and black dots depict $F_{\text{DNA,d}}$ with DNA protection using NaOAc of different concentrations as indicated. (b) $F_{\text{DNA,d}}$ (normalized by $F_{\text{DNA,d}}$ at $c_{\text{NaOAc}} = 0 \text{ M}$) versus c_{NaOAc} at fixed $c_{\text{H}_2\text{O}_2} = 0.87 \text{ mM}$ and $c_{\text{H}_2\text{O}_2} = 1.3 \text{ mM}$, respectively. The experimental data (dots) fit well with a sigmoidal curve (lines) resulting from a competition model discussed in the text. The IC_{50} value (half maximal inhibitory concentration), as displayed with the colored arrows, indicates the c_{NaOAc} concentration at which the effect of the radical attack is halved.

($k_{\text{DNA}} = 2 \times 10^9 \text{ M}^{-1} \text{ s}^{-1}$; cf. ref 2), the rate constant for the interaction of NaOAc with hydroxyl radicals can be extracted from eq 5. Based on the data of Figure 5a, we found rate constants of $k_{\text{NaOAc}} = 7.5 \times 10^7 \text{ M}^{-1} \text{ s}^{-1}$ at $c_{\text{H}_2\text{O}_2} = 0.87 \text{ mM}$ and $k_{\text{NaOAc}} = 3.9 \times 10^7 \text{ M}^{-1} \text{ s}^{-1}$ at $c_{\text{H}_2\text{O}_2} = 1.3 \text{ mM}$ (see Table S2 in the Supporting Information).

DISCUSSION

The effect of ROS on pBR322 is investigated by quantifying the amount of ssDNA and dsDNA before and after radical attack. After subjecting the DNA to hydroxyl radicals, it is immobilized onto PAH-functionalized mica, imaged by AFM tapping mode imaging and quantified by a height threshold data analysis.

Immobilization of the negatively charged DNA on a positively charged PAH layer was chosen as the strong electrostatic interaction prevents migration of the DNA chains on the substrate, which is observed in other approaches like immobilization based on multivalent ions.^{18,19} Moreover, as already four negative charges on a macromolecule are sufficient for its immobilization on a positively charge polyelectrolyte layer,²⁰ it is expected that PAH-based DNA immobilization allows the capture of even those DNA chains that are weakly charged due to the radical attack and are therefore hard to immobilize using multivalent ions.

We observed that PAH-based immobilization allowed determination of ssDNA and dsDNA strand heights with high reproducibility (see Supporting Information for details), which is a prerequisite for an analysis approach based on chain heights. Moreover, we found that 10–20% of the immobilized DNA adopted an open-circular conformation, which was larger than expected based on the specifications of the manufacturer claiming that the unattacked plasmid contains more than 95% supercoiled DNA and less than 3% open-circular DNA. Lyubchenko et al.²¹ show that the shape of tertiary structure of DNA is sensitive to the ionic conditions of the surrounding. The DNA was adsorbed under ambient conditions and without any buffer onto the PAH-functionalized mica surface. Thus, the carbon dioxide present in the air can dissolve into the solution of DNA, which may influence ionic strength and pH of the solution. Furthermore, the interaction of the DNA with the PAH-functionalized mica surface during the adsorption process itself may induce conformational change of the tertiary structure of the DNA. Additionally the indicated values were extracted from agarose gel measurements, which are rather volume than surface measurements as AFM tapping mode.

However, the small mismatch between the expected and measured fraction of the supercoiled DNA chains indicates that the PAH-based immobilization is sufficiently strong to allow reproducible DNA immobilization without drastically altering the chain conformation. Moreover, the ratio between supercoiled and open-circular DNA does not affect our quantification approach of DNA damage induced by free oxygen radicals. Both tertiary structures of DNA consist of dsDNA having the same height after adsorption to PAH-functionalized mica.

During the data analysis, the identification of dsDNA (intact DNA) and ssDNA (damaged DNA) is done based on the height of the DNA chains. For dsDNA, we measured a height of $5.2 \text{ \AA} \pm 0.6 \text{ \AA}$, which agrees with the height values in the literature for the plasmid pBR322.^{22–24} The measured height of ssDNA in this work is $2.3 \text{ \AA} \pm 0.4 \text{ \AA}$, which is slightly less than half of the height of dsDNA but agrees well with the height ratios between dsDNA and ssDNA reported in the literature.¹²

However, from the AFM images we determine DNA chain widths (full width at half-maximum)^{10,23} of $7.1 \text{ nm} \pm 1.1$ and $7.8 \text{ nm} \pm 1.2 \text{ nm}$ for ssDNA and dsDNA, respectively, which is larger than expected for a helical DNA structure (in which width and height of a cylindrical DNA chain should have the same values). This apparent contradiction can be solved by considering the tip convolution of the imaging process. The used cantilevers (OMCL-AC160TS) have typically a curvature radius around $r_c \cong 8 \text{ nm}$ (as determined by imaging of reference samples), which leads to a theoretical tip convoluted chain width of $4 \text{ nm} \pm 0.8$ and $6 \text{ nm} \pm 1 \text{ nm}$ for ssDNA and dsDNA, respectively.²²

Based on the differences in ssDNA and dsDNA height, in this work the quantification of the DNA damage (causing a transition from dsDNA to ssDNA) takes only the fraction of damaged DNA into account (eq 2); absolute DNA areas are not taken into account. This concept was applied by quantifying ROS-induced DNA modifications in the absence and presence of ROS scavengers and yielded competition curves for the interaction of DNA and sodium acetate, a known ROS scavenger, with hydroxyl radicals. The obtained IC_{50} values are in good agreement with the literature. For example, Peak et al. investigated sodium acetate as a scavenger for hydroxyl radicals induced by neutron irradiation, interacting with DNA ($c_{\text{DNA}} = 0.19 \text{ mM}$).²⁵ They found a decrease of

about 80% in single- and double-strand breaks at a sodium acetate concentration of 100 mM. A direct comparison of our data with this observation is difficult as the radical concentration is not exactly given in the original publication. However, Peak et al. quantify the relation between neutron irradiation and caused DNA damage, which allows us to roughly estimate the equivalent H_2O_2 concentration to be on the order of 1 mM, very similar to our experiments. Hence, taking our data into consideration ($c_{\text{DNA}} = 0.12 \text{ mM}$), the theoretical value for $F_{\text{DNA,d}}$ corresponding to the competition model at $c_{\text{NaOAc}} = 100 \text{ mM}$ is $F_{\text{DNA,d}} = 18\%$ (for $c_{\text{H}_2\text{O}_2} = 1.3 \text{ mM}$) or $F_{\text{DNA,d}} = 9\%$ (for $c_{\text{H}_2\text{O}_2} = 0.87 \text{ mM}$), which equals a decrease in DNA damage by 82% or 91%, respectively, being in good agreement with Peak et al.

However, NaOAc is known to quench hydroxyl radicals with a rate constant of $k = 7 \times 10^7 \text{ M}^{-1} \text{ s}^{-1}$.²⁶ Using a simple competition model we found rate constants of $k_{\text{NaOAc}} = 3.9 \times 10^7 \text{ M}^{-1} \text{ s}^{-1}$ and $k_{\text{NaOAc}} = 7.5 \times 10^7 \text{ M}^{-1} \text{ s}^{-1}$ for $c_{\text{H}_2\text{O}_2} = 1.3 \text{ mM}$ and 0.87 mM, respectively. Hence, our rate constants are in good agreement with the literature values, which demonstrates the applicability of this method of quantification of DNA damage. As explained in Materials and Method the height threshold based method of quantifying DNA damage introduced in this work only distinguishes between ssDNA and dsDNA. In past decades many other methods have been developed to quantify DNA damage. A group of analysis methods aims to detect ROS-induced chemical changes within the DNA chains. A well-established technique of this group is the HPLC method (high-performance liquid chromatography) coupled with tandem mass spectrometry.^{27,28} This method allows the quantification of ROS induced formation of nucleotide alterations within DNA chains. Since this method is able to detect one lesion in 10^6 normal base pairs, it is one of the most sensitive chemical methods.²⁹ However, these approaches have a relatively high material consumption (several 10 µg of DNA is required for analysis, see Table S2 in the Supporting Information), generally require DNA hydrolyzation prior analysis, and are not able to resolve changes in the tertiary structure of the DNA strands, which are known to have high potential to enhance mutagenicity.³

However, other DNA damage analysis methods are able to detect ROS-induced conformational changes of DNA tertiary structures. Among them gel electrophoresis is a well-established method, which enables the classification of intact and damaged DNA according to its geometry and size. This very sensitive method allows detecting as low as a few damaged base pairs per 10^9 normal base pairs.^{9,30,31} However, as the migration behavior of the DNA strands within the gel depends on a multitude of strand properties (e.g., strand length, conformation, charge, etc.), the interpretation of gel measurements of heterogeneous DNA samples (which is usually the case after ROS attack) is very challenging.

It is therefore straightforward to employ single molecule techniques like AFM imaging to analyze such heterogeneous DNA samples on the level of single DNA strands. Some of these AFM-based approaches separate intact and damaged DNA considering DNA double strand breaks and the following conformational transition of supercoiled and open circular DNA into linear DNA.^{11,32} Other approaches rely on the separation of intact and damaged DNA by the numbers of nodes of a single DNA molecule.¹⁰ This means that a DNA molecule is considered to be defective if the number of visible

crossover points is less than a typical threshold.³³ Here, we use the height difference of dsDNA and ssDNA to (indirectly) estimate changes in the tertiary structure rather than trying to (directly) quantify the numbers of DNA strands having a certain conformation or numbers of nodes. This has the advantage that it drastically simplifies the data analysis, as a categorization based on height information is much faster and more robust than approaches to determine the (lateral) conformation of DNA strands. The latter always requires tracing of the course of the strands on the supporting surface, which is time-consuming and challenging to automatize. The increase in data throughput is demonstrated in this study by analyzing the effect of sodium acetate, a known radical scavenger, and by retrieving its rate constant for the interaction with hydroxyl radicals.

CONCLUSIONS

A new approach to quantify ROS-induced DNA damage from AFM imaging of DNA strands was presented. In contrast to related studies, our approach is based on the height difference of single and double stranded DNA chains, which allows calculation of the fraction of areas occupied by intact and damaged DNA strands directly from the AFM images. Hence, only those kinds of DNA damage are quantified that cause a transition from double to single strands. The analysis is easy to implement and highly automatized, enabling high data throughput, which is demonstrated by investigating the competition of sodium acetate, a known ROS scavenger, with DNA with respect to their reaction with hydroxyl radicals. The respective competition curves resulted in the calculation of the rate constant for the interaction of sodium acetate with hydroxyl radicals, underlining the applicability of the presented approach for the study of complex interplay of ROS, ROS scavengers, and DNA. In comparison with the chemical information on DNA damage from HPLC methods (length scale $\approx 1 \text{ \AA}$) and the alteration within the tertiary DNA structure (gel electrophoresis, length scale $\gg 1 \text{ \AA}$), the measured information on this work (transition of dsDNA into ssDNA, length scale $\approx 4 \text{ nm}$ to $1.5 \mu\text{m}$) delivers a complementary view of DNA damage due to ROS.

ASSOCIATED CONTENT

Supporting Information

All determined rate constants for the interaction of sodium acetate with hydroxyl radicals are given. This material contains a detailed protocol of the sample preparation and a comparison of the amount of DNA required for the different methods usually employed for investigating ROS-induced DNA damage. Moreover, details on the reproducibility of the DNA height measurement and on the determination of the accuracy in extracting the single stranded DNA fraction and a discussion of nonuniform DNA damage are given. This material is available free of charge via the Internet at <http://pubs.acs.org>.

AUTHOR INFORMATION

Corresponding Authors

*Department of Applied Physics, Chalmers University of Technology, Fysikgränd 3, S-412 96 Gothenburg, Sweden. E-mail: stephan.block@chalmers.se.

*Institut für Physik, Ernst-Moritz-Arndt Universität, Felix-Hausdorff-Str. 6, D-17487 Greifswald, Germany, E-mail: helm@uni-greifswald.de.

Notes

The authors declare no competing financial interest.

ACKNOWLEDGMENTS

Financial support of the Graduate School “Studies of the interaction of free oxygen radicals with molecules at electrodes and applications to biochemical and medical systems” of the Alfried Krupp Wissenschafts Kolleg Greifswald, the European Social Fund (Grant No. UG 10 022), the state of Mecklenburg-Vorpommern and within the Research Training Group (GRK) 1947, project B1, is gratefully acknowledged.

REFERENCES

- (1) Marnett, L. J. Oxyradicals and DNA damage. *Carcinogenesis* **2000**, *21* (3), 361–370.
- (2) Dizdaroglu, M.; Jaruga, P.; Birincioglu, M.; Rodriguez, H. Free radical-induced damage to DNA: mechanisms and measurement. *Free Radical Biol. Med.* **2002**, *32* (11), 1102–1115.
- (3) Cooke, M. S.; Evans, M. D.; Dizdaroglu, M.; Lunec, J. Oxidative DNA damage: mechanisms, mutation, and disease. *FASEB J.* **2003**, *17* (10), 1195–1214.
- (4) Kryston, T. B.; Georgiev, A. B.; Pissis, P.; Georgakilas, A. G. Role of oxidative stress and DNA damage in human carcinogenesis. *Mutat. Res.* **2011**, *711* (1), 193–201.
- (5) Jacob, C., Winyard, P. G., Eds. *Redox signaling and regulation in biology and medicine*; John Wiley & Sons: 2009.
- (6) Ishimura, Y.; Nozaki, M.; Yamamoto, S.; Shimizu, T.; Narumiya, S.; Mitani, F. *Oxygen and Life: Oxygenases, Oxydases and Lipid Mediators*; Excerpta Medica. International Congress Series 1233; Elsevier: 627 Amsterdam, 2002.
- (7) Malins, D. C.; Polissar, N. L.; Gunselman, S. J. Progression of human breast cancers to the metastatic state is linked to hydroxyl radical-induced DNA damage. *Proc. Natl. Acad. Sci. U.S.A.* **1996**, *93* (6), 2557–2563.
- (8) Dizdaroglu, M.; Jaruga, P. Mechanisms of free radical-induced damage to DNA. *Free Radical Res.* **2012**, *46* (4), 382–419.
- (9) Sutherland, B. M.; Georgakilas, A. G.; Bennett, P. V.; Laval, J.; Sutherland, J. C. Quantifying clustered DNA damage induction and repair by gel electrophoresis, electronic imaging and number average length analysis. *Mutat. Res.* **2003**, *531* (1), 93–107.
- (10) Jiang, Y.; Ke, C.; Mieczkowski, P. A.; Marszałek, P. E. Detecting ultraviolet damage in single DNA molecules by atomic force microscopy. *Biophys. J.* **2007**, *93* (5), 1758–1767.
- (11) Boichot, S.; Fromm, M.; Cunniffe, S.; O'Neill, P.; Labrune, J. C.; Chambaudet, A.; Delain, E.; Le Cam, E. Investigation of radiation damage in DNA by using atomic force microscopy. *Radiat. Prot. Dosim.* **2002**, *99* (1–4), 143–146.
- (12) Adamcik, J.; Klinov, D. V.; Witz, G.; Sekatskii, S. K.; Dietler, G. Observation of single-stranded DNA on mica and highly oriented pyrolytic graphite by atomic force microscopy. *FEBS Lett.* **2006**, *580* (24), 5671–5675.
- (13) Berg, F.; Block, S.; Drache, S.; Hippler, R.; Helm, C. A. Effects of reactive oxygen species on single polycation layers. *J. Phys. Chem. B* **2013**, *117* (28), 8475–8483.
- (14) Gröning, A.; Ahrens, H.; Ortmann, T.; Lawrenz, F.; Brezesinski, G.; Scholz, F.; Helm, C. A. Molecular mechanisms of phosphatidylcholine monolayer solidification due to hydroxyl radicals. *Soft Matter* **2011**, *7* (14), 6467–6476.
- (15) Zhang, J.; McCauley, M. J.; Maher, L. J.; Williams, M. C.; Israeloff, N. E. Mechanism of DNA flexibility enhancement by HMGB proteins. *Nucleic Acids Res.* **2009**, *37* (4), 1107–1114.
- (16) Onoa, G. B.; Moreno, V. Study of the modifications caused by cisplatin, transplatin, and Pd (II) and Pt (II) mepirizole derivatives on pBR322 DNA by atomic force microscopy. *Int. J. Pharm.* **2002**, *245* (1), 55–65.
- (17) Hill, A. V. The possible effects of the aggregation of the molecules of haemoglobin on its dissociation curves. *J. Physiol. (London)* **1910**, *40*, 4–7.

- (18) Bustamante, C.; Vesenka, J.; Tang, C. L.; Rees, W.; Guthold, M.; Keller, R. Circular DNA molecules imaged in air by scanning force microscopy. *Biochemistry* **1992**, *31* (1), 22–26.
- (19) Shlyakhtenko, L. S.; Gall, A. A.; Weimer, J. J.; Hawn, D. D.; Lyubchenko, Y. L. Atomic force microscopy imaging of DNA covalently immobilized on a functionalized mica substrate. *Biophys. J.* **1999**, *77* (1), 568–576.
- (20) Radtchenko, I. L.; Sukhorukov, G. B.; Leporatti, S.; Khomutov, G. B.; Donath, E.; Möhwald, H. Assembly of alternated multivalent ion/polyelectrolyte layers on colloidal particles. Stability of the multilayers and encapsulation of macromolecules into polyelectrolyte capsules. *J. Colloid Interface Sci.* **2000**, *230* (2), 272–280.
- (21) Lyubchenko, Y. L.; Shlyakhtenko, L. S. Visualization of supercoiled DNA with atomic force microscopy *in situ*. *Proc. Natl. Acad. Sci. U.S.A.* **1997**, *94* (2), 496–501.
- (22) Liu, Z.; Li, Z.; Zhou, H.; Wei, G.; Song, Y.; Wang, L. Immobilization and condensation of DNA with 3-aminopropyltriethoxysilane studied by atomic force microscopy. *J. Microsc.* **2005**, *218* (3), 233–239.
- (23) Liu, Z.; Li, Z.; Zhou, H.; Wei, G.; Song, Y.; Wang, L. Imaging DNA molecules on mica surface by atomic force microscopy in air and in liquid. *Microsc. Res. Tech.* **2005**, *66* (4), 179–185.
- (24) Seitz, E. M.; Brockman, J. P.; Sandler, S. J.; Clark, A. J.; Kowalczykowski, S. C. RadA protein is an archaeal RecA protein homolog that catalyzes DNA strand exchange. *Genes Dev.* **1998**, *12* (9), 1248–1253.
- (25) Peak, J. G.; Ito, T.; Robb, F. T.; Peak, M. J. DNA damage produced by exposure of supercoiled plasmid DNA to high-and low-LET ionizing radiation: effects of hydroxyl radical quenchers. *Int. J. Radiat. Biol.* **1995**, *67* (1), 1–6.
- (26) Minakata, D. Development of aqueous phase hydroxyl radical reaction rate constants predictors for advanced oxidation processes. PhD thesis, Georgia Institute of Technology, 2010.
- (27) Cadet, J.; Douki, T.; Gasparutto, D.; Ravanat, J. L. Oxidative damage to DNA: formation, measurement and biochemical features. *Mutat. Res.* **2003**, *531* (1), 5–23.
- (28) Cadet, J.; Weinfeld, M. Detecting DNA damage. *Anal. Chem.* **1993**, *65* (15), 675A–682A.
- (29) Cadet, J.; Delatour, T.; Douki, T.; Gasparutto, D.; Pouget, J. P.; Ravanat, J. L.; Sauvage, S. Hydroxyl radicals and DNA base damage. *Mutat. Res.* **1999**, *424* (1), 9–21.
- (30) Blazek, E. R.; Peak, M. J. The role of hydroxyl radical quenching in the protection by acetate and ethylenediaminetetraacetate of supercoiled plasmid DNA from ionizing radiation-induced strand breakage. *Int. J. Radiat. Biol.* **1988**, *53* (2), 237–247.
- (31) Sutherland, B. M.; Bennett, P. V.; Sidorkina, O.; Laval, J. Clustered DNA damages induced in isolated DNA and in human cells by low doses of ionizing radiation. *Proc. Natl. Acad. Sci. U.S.A.* **2000**, *97* (1), 103–108.
- (32) Su, M.; Yang, Y.; Yang, G. Quantitative measurement of hydroxyl radical induced DNA double-strand breaks and the effect of N-acetyl-l-cysteine. *FEBS Lett.* **2006**, *580* (17), 4136–4142.
- (33) Bussiek, M.; Mücke, N.; Langowski, J. Polylysine-coated mica can be used to observe systematic changes in the supercoiled DNA conformation by scanning force microscopy in solution. *Nucleic Acids Res.* **2003**, *31* (22), e137–e137.